

Article

Energy Converter with Inside Two, Three, and Five Connected H₂/Air Swirling Combustor Chambers: Solar and Combustion Mode Investigations

Angelo Minotti

Department of Astronautic, Electrics & Energetics Engineering, University of Rome “La Sapienza” Via Eudossiana 18, Rome 00184, Italy; angelo.minotti@uniroma1.it; Tel.: +39-328-289-1745

Academic Editor: George Kosmadakis

Received: 7 December 2015; Accepted: 8 June 2016; Published: 17 June 2016

Abstract: This work reports the performance of an energy converter characterized by an emitting parallelepiped element with inside two, three, or five swirling connected combustion chambers. In particular, the idea is to adopt the heat released by H₂/air combustion, occurring in the connected swirling chambers, to heat up the emitting surfaces of the thermally-conductive emitting parallelepiped brick. The final goal consists in obtaining the highest emitting surface temperature and the highest power delivered to the ambient environment, with the simultaneous fulfillment of four design constraints: dimension of the emitting surface fixed to 30 × 30 mm², solar mode thermal efficiency greater than 20%, emitting surface peak temperature $T > 1000$ K, and its relative $\Delta T < 100$ K in the combustion mode operation. The connected swirling meso-combustion chambers, inside the converter, differ only in their diameters. Combustion simulations are carried out adopting 500 W of injected chemical power, stoichiometric conditions, and detailed chemistry. All provide high chemical efficiency, $\eta > 99.9\%$, and high peak temperature, but the emitting surface ΔT is strongly sensitive to the geometrical configuration. The present work is related to the “EU-FP7-HRC-Power” project, aiming at developing micro-meso hybrid sources of power, compatible with a thermal/electrical conversion by thermo-photovoltaic cells.

Keywords: meso-combustor; hydrogen-air combustion; whirl flow; fluid-structure interaction; computational fluid dynamics; detailed chemistry

1. Introduction

The always-increasing energy demand imposes the investigation of new form of energy supply, which must match with some fundamental requirements, such as:

- (1) Providing reliable and continuous base-load power;
- (2) Providing peak-load power when needed;
- (3) Being the “greenest” possible; and
- (4) Being tailored according to the different necessities.

Renewable energies reply surely to the previous point 3, but their intermittent nature has a large impact in terms of low capacity factors, low flexibility, and amortization costs.

Probably the only path to follow is, therefore, the integration of different technologies, in order to use them, separately or simultaneously, according to the actual necessities and conditions.

The “HRC-Power” project (Hybrid Renewable energy Converter for continuous and flexible Power production) aims at replying all the aforementioned requirements, integrating both combustion and solar concentration modes, into miniaturized items.

Miniaturization, mandatory for a device with the aim of being usable even for very small energy demands, imposes strategies to overcome the typical drawbacks of miniaturized combustion systems; that is, incomplete combustion and flame instability [1].

In the light of the above, the HRC-Power project designs the integration of a parallelepiped brick, characterized by emitting walls, with internal micro-meso swirling combustion chambers (this integration is under a pending patent [2]).

The parallelepiped brick delivers, to the external ambient environment, thermal energy via the emitting walls that are heated up by the sun and/or by the heat released during the chemical combustion taking place inside the swirling combustion chambers.

That thermal energy is finally converted into electrical energy by a thermo-photovoltaic system (TPV).

The real potentialities of this integration are analyzed in [1]. In particular, numerical simulation of a parallelepiped emitting brick with two internal micro-meso swirling chambers, fed by H₂/air with 400 W of injected thermal power, at different equivalence ratios and with different chamber diameters, are carried out.

Results were encouraging in terms of delivered power and of peak surface temperature.

Once demonstrated, with the work in [1], that the overall system would work properly, new and more specific design requirements have been defined in order to make the overall micro-system compatible with a thermal/electrical conversion by thermo-photovoltaic cells.

The new design requirements were:

- The emitting surface dimensions equal to 30 × 30 mm;
- The converter thermal resistance efficiency, in the solar mode operation, $\eta_{TR} \geq 20\%$ (see Equation (1));
- The peak temperature on the emitting surface, in the combustion mode operation, $T_{\text{peak emitting surface}} > 1000$ K; and
- The delta temperature on the emitting surface, in the combustion mode, $\Delta T_{\text{emitting surface}} < 100$ K.

Novel geometrical configurations were defined to fulfill the project constraints and the purpose of the present paper is to present them with the relative investigations.

The novelty consists in the integration of an emitting parallelepiped and two, three, and five connected swirling chambers. The “connected chambers configuration” has been chosen to increase the overall residence time and to balance the cold and hot points on the emitting surfaces, with the goal of reducing the emitting surfaces delta-temperature.

That three connected configurations, which differ in the chamber diameters (the chamber’s length is fixed at 33 mm), are *in primis* investigated by means of a thermal resistance efficiency analysis to mimic the solar mode operation (see Section 3).

This analysis has been carried out to understand how the combustion chamber holes, inside the converter, affect the thermal conduction from the top wall, which faces the sun, to the bottom one that faces the TPV.

It is important to highlight that the area of the emitting surface (the one that faces the TPV cells) has been made fixed and only the thickness of the converter changed with the different length/diameter Z/D ratios. In fact, the dimensions of the converters in the 2-3-5 connected chambers configurations are, respectively 30 × 30 × 6 mm³, 30 × 30 × 9 mm³, and 30 × 30 × 14 mm³.

After the solar mode investigation, combustion simulations are carried out. They assume stoichiometric conditions, 500 W of total chemical injected power, and detailed chemistry (see Section 4).

Turbulence is modeled adopting the *k*- ϵ turbulence approach, while the eddy dissipation concept models the chemistry-turbulence coupling (see Section 4.2).

Results are reported in Section 4.3, with a special focus on the chemical efficiency values, fluid-structure interaction, temperature distribution on the emitting surfaces, and thermal power delivered to the external ambient environment.

There are no available studies that consider connected swirling chambers in such small devices.

This work is part of the outcomes of the “European FP7-HRC Power” project (cordis.europa) [3]. The main purpose of the HRC project is the development of hybrid sources of power (Harnessing hybrids, Pan European Networks) [4].

2. Energy Converter

The energy converter is represented in Figure 1; it shows, separately, a swirling chamber, a thermally-conductive parallelepiped brick and their relative integration into the energy converter itself (overall dimensions are reported in Figures 2–4).

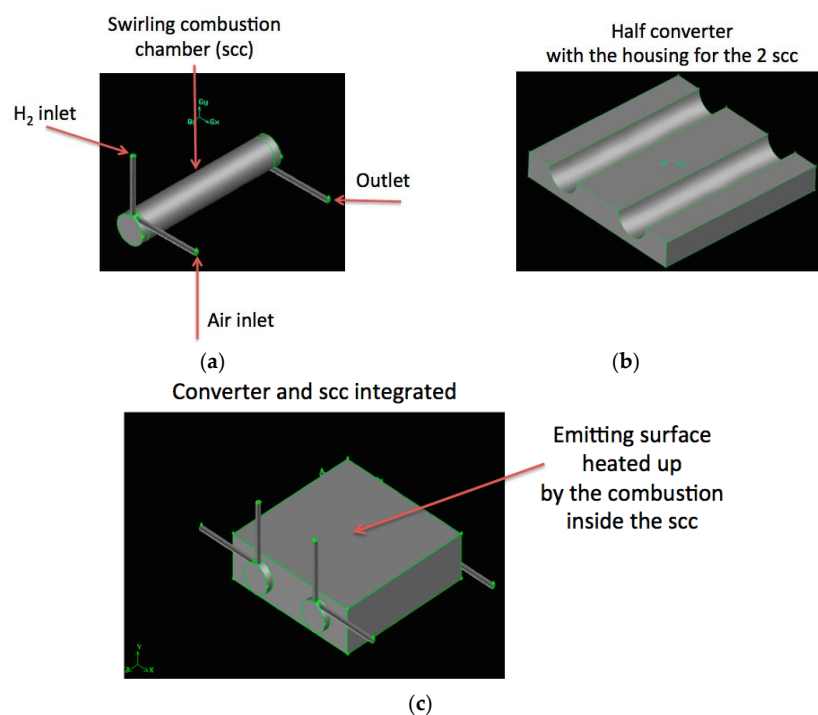


Figure 1. Swirling chamber (a); half thermal conductive brick (b); and integration into the energy converter (c).

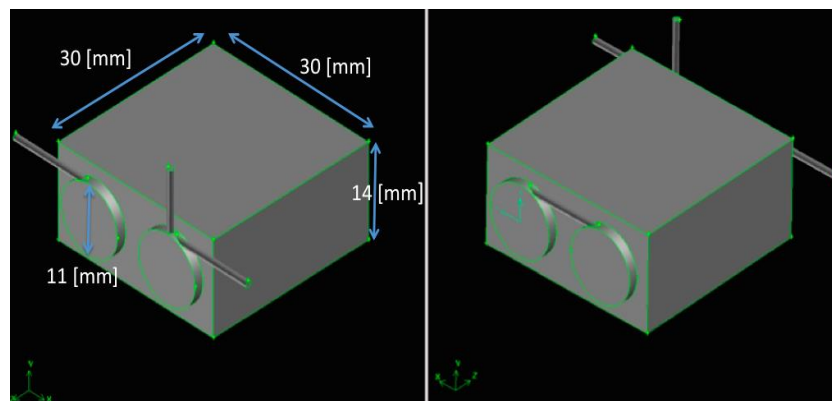


Figure 2. Swirling combustor converter, $Z/D = 3$, 2 connected chambers.

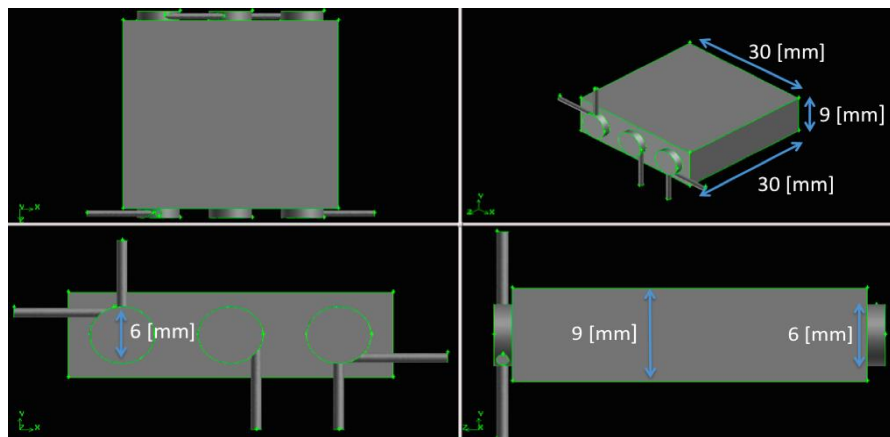


Figure 3. Swirling combustor converter, $Z/D = 5$, 3 connected chambers.

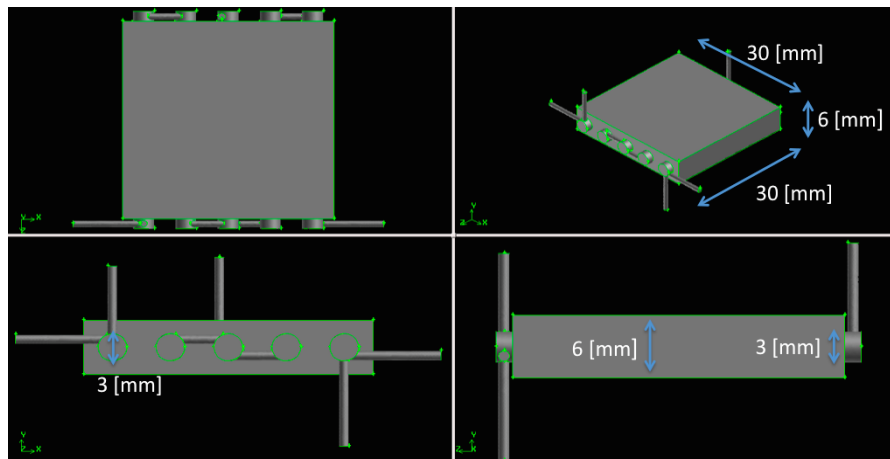


Figure 4. Swirling combustor converter, length/diameter ratio (Z/D) = 11, 5 connected chambers.

The gaseous fuel (hydrogen) is injected into the combustion chamber in the radial direction, at 90° with respect to the air flow, to improve mixing and to generate the swirling motion which is enhanced by the higher air kinetic energy, injected tangentially. Both air and fuel injection orifices, together with the exhaust duct, are 1 mm in diameter to ease the drilling phase. Gases exhaust in the tangential direction, and this geometrical solution enhances mixing by the definition of recirculation bubbles [5].

The internal chamber walls are coupled with the SiC block; this permits heating of the block itself and then delivering thermal power to the environment by its external walls (through convection and radiation).

The technological requirements (emitting surface dimension equal to $30 \times 30 \text{ mm}^2$; converter thermal resistance efficiency, during the solar mode, $\eta_{\text{TR}} \geq 20\%$, $T_{\text{peak emitting surface}} > 1000 \text{ K}$; and $\Delta T_{\text{emitting surface}} < 100 \text{ K}$ during the combustion mode), and the results reported in [1], imposed the definition of new geometrical configurations.

The new configurations are characterized by two, three, and five connected swirling combustion chambers, inside the emitting parallelepiped element; see Figures 2–5, for the geometrical configuration and the relative overall dimensions.

The combustion chambers, adopted in the three configurations, differ for their diameters (3–6–11 mm) while the axial length is fixed to 33 mm. Consequently, they are characterized by different aspect ratios ($Z/D = 11$ –5–3) and by different total combustion volumes (about 1166–2798–6269 mm^3). The converters have x - z fixed dimensions ($30 \times 30 \text{ mm}^2$), while the thickness (y -dimension) is always

3 mm greater than the diameter, then 6-9-14 mm; the relative distance between the chambers is 4-4-3 mm. These geometrical characteristics are reported in the following Table 1.

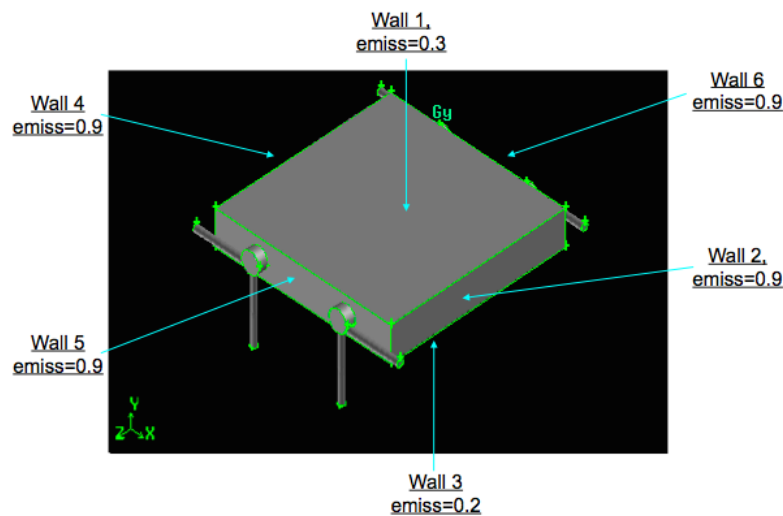


Figure 5. Swirling combustor converter, $Z/D = 11-5$ chambers, emissivity values.

Table 1. Converters, geometrical characteristics.

Aspect Ratio Z/D	Chamber Diameter (mm)	Number of Chambers	Chamber Length (mm)	Brick Dimensions $L \times W \times$ T (mm)	Distance between the Chambers (mm)	Chambers' Volume (mm^3)
11	3	5	33	$30 \times 30 \times 6$	3	1166
5	6	3	33	$30 \times 30 \times 9$	4	2798
3	11	2	33	$30 \times 30 \times 14$	4	6269

The $Z/D = 5-11$ configurations present two fuel inlet ducts and one outlet duct, while the $Z/D = 3$ presents only one fuel inlet duct. The connections, among the chambers, permit to increase the overall residence time (it increases the total available volume) and to balance the cold and hot points on the emitting surfaces.

These three configurations have been analyzed, *in primis*, by means of solar mode simulations (see Section 3) and, the ones that fulfill the thermal resistance efficiency requirement ($\eta_{TR} \geq 20\%$), are investigated adopting reactive Navier-Stokes simulations (see Section 4 for numerical details and results).

3. Solar Mode Simulations

A Fourier parametric analysis has been carried out to mimic the solar mode operation to understand the effects of the dimensions of the chambers' diameters, inside the converter, on the converter's thermal conductivity and, consequently, on the final TPV energy conversion.

As previously described, the three configurations differ in the chamber diameters, in their number and then in the converter's thickness. Solar mode simulations are carried out imposing a thermal flux of about 500 W on the "wall 1" ("wall 1" is the surface that faces the sun, see Figure 5).

This value is reached by defining an external radiative source, which mimics the sun, at a temperature of about 2600 K.

The walls are emitting surfaces, according to the emissivity values reported in Figure 5.

The walls are characterized by a convective coefficient $H = 12 \text{ W}/(\text{m}^2 \times \text{K})$, calculated at standard and rest conditions. Chamber walls are thermally conductive, while inlet and exhaust ducts walls are adiabatic (to mimic a material with insulating properties).

The parallelepiped is modeled adopting the following material properties:

- Density, $\rho = 3100 \text{ kg/m}^3$;
- Specific heat at constant pressure, $C_p = 600 \text{ J}/(\text{kg} \times \text{K})$; and
- Thermal conductivity, according to the polynomial reported in [6].

Investigations have been carried out analyzing the thermal resistance efficiency according to the following Equation (1):

$$\eta_{TR} = \left| \frac{\text{delivered thermal power [W]}_{\text{wall 3}}}{\text{absorbed thermal power [W]}_{\text{wall 1}}} \right| \quad (1)$$

Results are reported in the following Table 2.

Table 2. Solar mode investigations: results.

Aspect Ratio Z/D	Number of Chambers	External Radiation Temperature (K)	Heat Transfer Wall 1 (W)	Heat Transfer Wall 3 (W)	Thermal Resistance Efficiency η_{TR}
11	5	2600	488 ¹	-130	26.64
5	3	2600	512	-102	19.92
3	2	2600	530	-72	13.58

¹ Thermal power on “wall 1” is positive in sign because it is absorbed by the environment (the sun), while the one related to “wall 3” is negative because it is released to the ambient environment.

The solar mode investigation indicates that the $Z/D = 3$ configuration (two chambers; 11 mm in diameter; 14 mm of total thickness) exceeds the 20% thermal resistance efficiency limit, while the $Z/D = 5$ and $Z/D = 11$ configurations (respectively, three chambers; 6 mm of diameter; 9 mm of total thickness, and five chambers; 3 mm of diameter; 6 mm of total thickness) fulfill the thermal resistance efficiency constraint, even though the $Z/D = 5$ is at the limit.

Figures 6 and 7 report the thermal maps in the solar mode operation for the $Z/D = 5-11$ configurations.

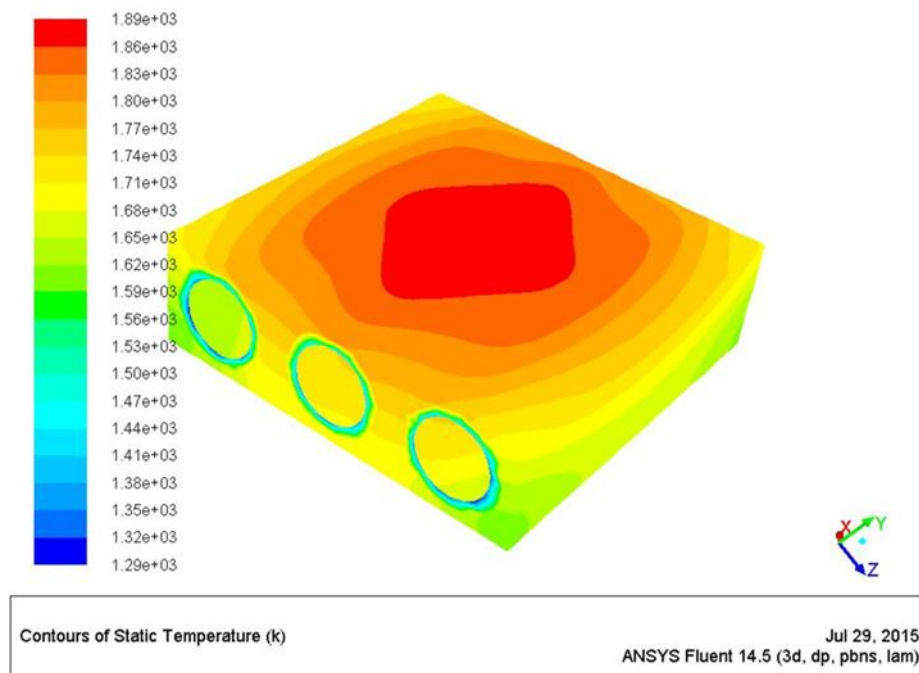


Figure 6. Thermal map, $Z/D = 5$, solar mode.

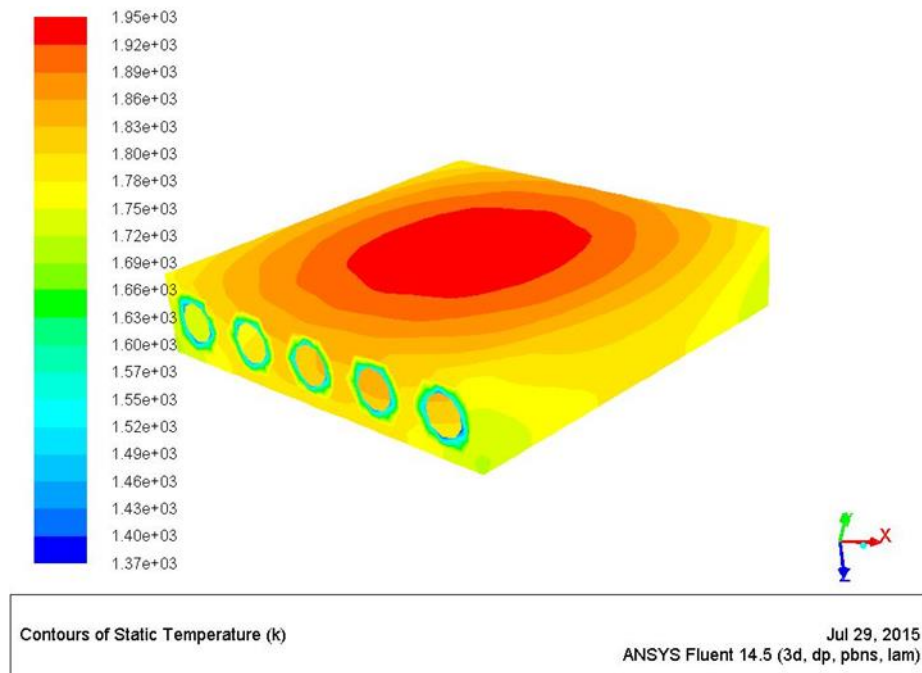


Figure 7. Thermal map, $Z/D = 11$, solar mode.

In light of the previous results, combustion simulations are carried out only for the $Z/D = 11$ and $Z/D = 5$ configurations; see the following Section 4.

4. Combustion Mode Simulations

In this section the reactive Navier-Stokes numerical simulations are reported. The aim is to obtain the maximum peak temperature, the smallest ΔT , and the maximum thermal power, delivered to the environment, from the emitting wall that faces the TPV.

In particular, section 4.1 describes the operating conditions, Section 4.2 the numerical modeling, and Section 4.3 the results.

4.1. Operating Conditions

Investigations are carried out assuming 500 W of injected thermal power at stoichiometric conditions and adopting inlet temperature equal to 450 K, to mimic pre-heating at stationary conditions. The inlet mass flows and the relative Reynolds numbers are shown in Table 3.

Table 3. Operating conditions.

Aspect Ratio Z/D *	Total Injected Chemical Power [W] (H_2/Air kg)	Phi	Re (Fuel-Air)
11-5 chambers	500 ($4.16 \times 10^{-6}/2.043 \times 10^{-4}$)	1	240-5300
5-3 chambers	500 ($4.16 \times 10^{-6}/2.043 \times 10^{-4}$)	1	240-5300

* Z is fixed at 33 mm for all of the configurations.

The inlet Reynolds numbers, respectively laminar and turbulent for the fuel and air inlets, impose deeper investigations to understand whether the flow is fully turbulent or not (Reynolds numbers are based on the 1 mm orifice diameter); laminar and moderately turbulent flow regimes are a typical feature of micro-meso combustor [7].

The regime depends on temperature (viscosity increases with the root of the temperature), on the expansion effects inside the chamber and on the complex fluid dynamics that characterizes these small devices (swirling and recirculation motions).

These considerations explain the fact that laminar zones may locally exist together with turbulent zones and *vice versa*, introducing the issue of which approach should be chosen to solve the reactive Navier-Stokes equations; see Sections 4.2 and 4.3 for further details.

The swirl number (S_w) is the result of the air-fuel injections parameters and geometry; it is defined as the axial flux of the swirling momentum divided by the axial flux of the axial momentum (see Equation (2)):

$$S_w = \frac{\int_A \rho u_z u_\theta r dA}{r \int_A \rho u_z^2 dA} \quad (2)$$

The surface integral is calculated at the $Z = 0.03$ m height, immediately downward of the inlet plane (S_w values, at reacting conditions, are reported in Section 4.3).

4.2. Numerical Modeling

The grid sensitivity analysis, reported in [1], indicated that a circumferential distance between gridpoints of 0.2 mm, on the chambers, and of 1 mm, on the walls of the brick, is the optimum. The meshes, adopted in the present study, have a total number of cells respectively equal to about 1.4 M (5 chambers)–2.2 M (3 chambers). The grid analysis carried out at cold conditions is assumed suitable for the reacting case as well; this is because greater levels of turbulence, and then greater gradients, characterize cold conditions with respect to the same case at reacting conditions and, moreover, combustion is modeled by the EDC confirming the fact that it is the turbulence the focal issue

After this, “reordering, smoothing, and swapping” techniques were adopted for the three meshes in order to speed up calculations and increase mesh quality. In particular, reordering (the reverse Cuthill-McKee method [8]) was adopted to reduce the bandwidth of the cell neighbor number, in order to speed up the calculations, while “smoothing and swapping” were used, respectively, to reposition nodes (by lowering the maximum skewness of the grid) and to modify the cell connectivity.

The latter technique produces a constrained Delaunay mesh [9] in which the minimum angles in the mesh are maximized, tending toward equilateral cells, providing the “most equilateral” grid for the given node distribution.

The first point near the wall is at $y^+ < 3$ and $\Delta y^+ < 1$, for all of the configurations (only a few points, in the air inlet ducts where velocities are higher, are close to $y^+ \sim 15$). This means that the first point away from the wall is inside the viscous sublayer.

As previously mentioned, laminar zones may coexist with turbulent ones inside micro-meso combustors. This poses the problem of which numerical model is the most reliable to treat this physical peculiarity.

A pure laminar approach would be unable to predict turbulent field zones, of crucial importance when reactions are present, while turbulent models would over-predict transport wherever the actual regime was laminar.

Fluid dynamics have been solved adopting the RANS k-eps turbulence approach, with the enhanced wall treatment [10].

This model has been chosen for its ability to reproduce laminar dynamics and for the fact that it solves the eps-unknown, which is present in the definition of the Kolmogorov scales, $\eta = \left(\frac{\nu^3}{\epsilon}\right)^{\frac{1}{4}}$.

The Kolmogorov scale provides an indication of the actual flow regime and permits understanding the feasibility of a direct numerical simulation (DNS) inside the chamber.

The specific heat at constant pressure, $C_{p,i}$, is fitted by polynomials of temperature from the GRIMEch Thermo Data file [11], properly introduced in the CFD code, while viscosity and thermal conductivity, μ and k , are predicted by the gas kinetic theory [12]; mixtures are composition-dependent according to Wilke’s formula [13].

The turbulence-combustion coupling is modeled adopting the eddy dissipation concept (EDC) [14,15], while the hydrogen/air kinetics are modeled with a detailed mechanism of nine species and 21 reactions [16].

The reactive Navier–Stokes equations were solved adopting a finite-volume solver (Ansys 14 CFD code). The computing resources, and the eventual related technical support, used for this work, is part of the CRESCO/ENEAGRID High Performance Computing infrastructure and its staff [17]. CRESCO/ENEAGRID High Performance Computing infrastructure is funded by ENEA, the Italian National Agency for New Technologies, Energy, and Sustainable Economic Development, and by Italian and European research programs [18].

The simulations were carried out adopting the pressure-based version of the solver, assuming the PISO scheme [19,20] to solve the pressure-velocity coupling and the third-order MUSCL scheme [21] for the spatial discretization of all the variables. Further investigations could also consider higher-order discretization algorithms, such as MUSCL fifth-order, WENO fifth-order, and/or WENO ninth-order [22], in particular with the LES or DNS approach.

4.3. Results and Discussion

In the literature, a numeric-experiment comparison related to swirling combustion chambers [9] is available. That investigation assumes methane with 123 W of injected thermal power, one swirling chamber ($6 \times 9 \text{ mm}^2$), 3 atm of operating pressure, and no fluid-structure interaction. Results confirmed a great correspondence between numerical and experimental combustion efficiency (84%–85%), confirming that the overall approach is correct.

In order to facilitate the discussion, the outcomes of the two final configurations ($Z/D = 5-11$) are reported in the following Tables 4 and 5. They provide the available volume, the combustion efficiency (Equation (3)), the average temperature at the exhaust section, the swirling number at reacting conditions (Equation (2), calculated at $Z = 30 \text{ mm}$), the maximum temperature, the minimum temperature, the average temperature, the standard deviation and, finally, the external heat transfer; these data are provided both for “wall 1” and “wall 3”.

Table 4. Overall results of the final configurations.

Aspect Ratio Z/D	Number of Chambers (Total Volume m^3)	Phi	Combustion Efficiency	Average Temperature at the Exhaust Section [K]	Swirling Number (Reacting Conditions)
11	5 (1.165×10^{-6})	1	>99.9%	1202	1.148
5	3 (2.797×10^{-6})	1	>99.9%	1186	2.082

Table 5. Overall results of the final configurations.

Aspect Ratio Z/D	External Heat Transfer Wall1-Wall 3 [W]	Wall 1 Tmax-Tmin [K]	Wall 1 Taverage- σ_T [K]	Wall 3 Tmax-Tmin [K]	Wall 3 Taverage- σ_T [K]
11	66-48	1389-1344	1374-8.36	1390-1345	1376-8.31
5	58-43	1342-1269	1322-15.6	1346-1271	1325-15.8

The iterative solution was assumed converged when the difference between the inlet and outlet mass flow rates, $\Delta m / \Delta t$, was at least two orders of magnitude smaller than the smallest flow rate at the inlet section (that is, the hydrogen injection).

$$\eta_{\text{combustion}} = \frac{H_{2_{\text{inlet}}} - H_{2_{\text{outlet}}}}{H_{2_{\text{inlet}}}} \quad (3)$$

The combustion efficiency data, reported in Table 4, indicate that the chemical efficiency is high for both of the configurations. In fact, the H_2 chemistry is fast enough to have complete combustion (chemical efficiency greater than 99%), even for the $Z/D = 11$ configuration (diameter equal to 3 mm).

The swirling number, S_w , correctly increases with the diameter, due to the decreased curvature, and then to the increased tangential velocity; this surely affects the “pushing effect” of the fresh reactants against the internal chamber wall, improving the thermal protection effect and increasing the residence time and the mixing.

The $Z/D = 11$ configuration provides greater thermal power to the ambient environment from both the walls; in fact, the maximum temperatures, the minimum temperatures, and the average ones, are greater than the respective ones obtained with the $Z/D = 5$ configuration.

This result is confirmed by the standard deviation that, in the $Z/D = 11$ configuration, is about half of that in the $Z/D = 5$ configuration.

Both of the configurations fulfill the required performance ($T_{\text{peak emitting surface}} > 1000$ K and $\Delta T_{\text{emitting surface}} < 100$ K). In fact, the $Z/D = 11$ ($Z/D = 5$) configurations reach, from the emitting surfaces “wall 3”, a peak temperature value equal to 1390 K (1346 K) and the $\Delta T = 45$ K ($\Delta T = 75$ K). These performances indicate that both of the configurations are compatible with a thermal/electrical conversion by thermo-photovoltaic cells.

Figure 8 reports the power delivered to the ambient from “wall 1” and “wall 3”, Figure 9 reports the maximum, minimum, and the average temperature on “wall 1” and “wall 3”, while Figure 10 reports the standard deviation, σ_T , of “wall 1” and “wall 3” (the results are provided as a function of the number of chambers inside the converter, which is inversely proportional to the chambers diameter dimension, to the total thickness and, finally, to the Z/D aspect ratio).

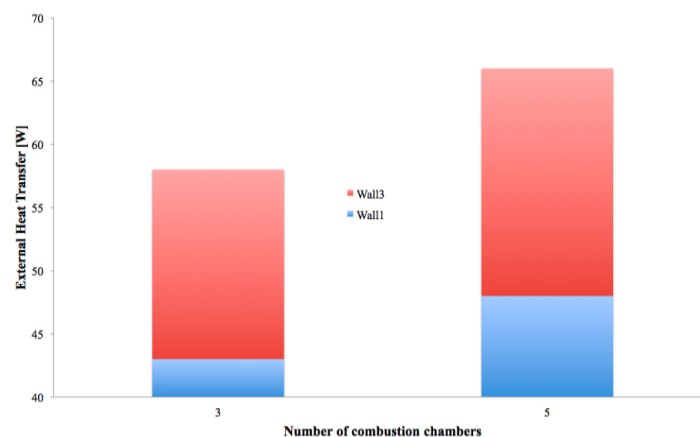


Figure 8. Power delivered to the ambient environment [W], “wall 1” and “wall 3”.

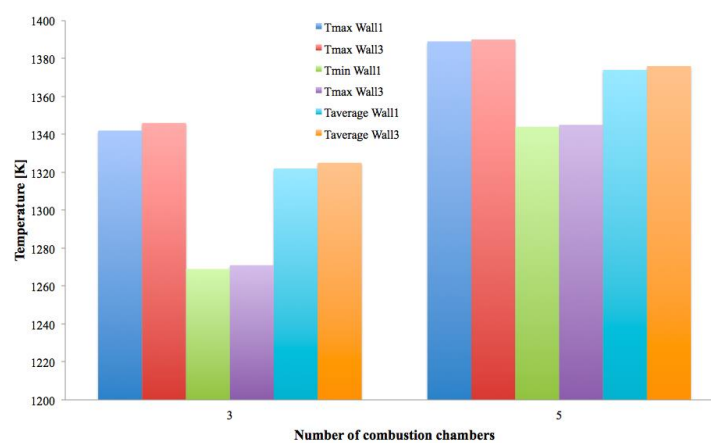


Figure 9. Minimum, maximum, and average temperature [K], “wall 1” and “wall 3”.

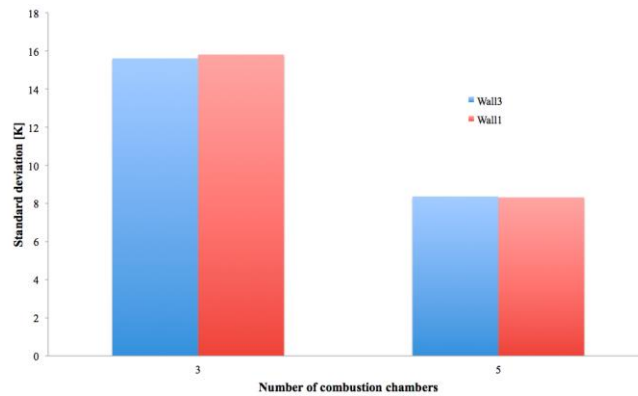


Figure 10. Standard deviation, “wall 1” and “wall 3”.

As in [1], this work confirms that defining a single regime inside the chamber would be incorrect, because the Kolmogorov scale, see Figure 11, identifies weak turbulence zones (in the air inlet ducts and in the first zones of the chambers) together with laminar ones (fuel inlets and inside the chambers).

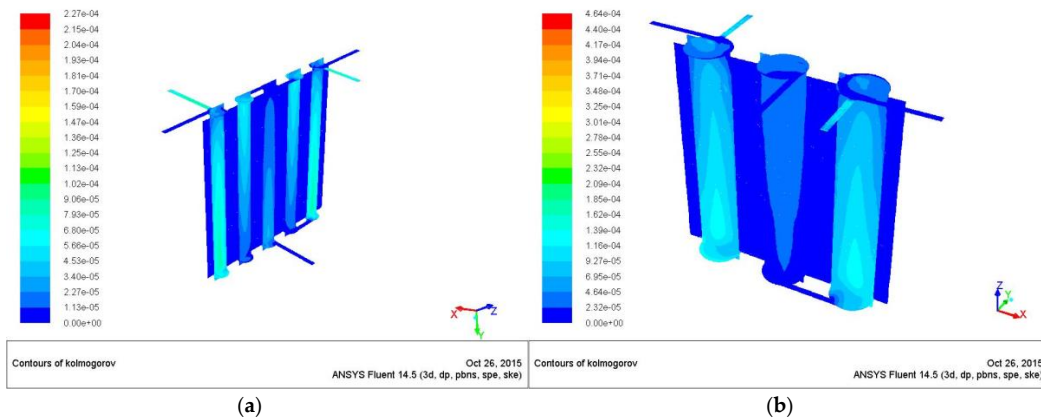


Figure 11. $Z/D = 11$ (a); and $Z/D = 5$ (b), Kolmogorov dimension.

Figure 12 presents the temperature map on the walls of the combustion. The effects of the two different wall boundary conditions (the adiabatic wall, at the inlet and outlet sections, and the conductive walls in the central part of the chambers) are evident. Figure 13 reports the temperature map on the meridian $x-z$ plane, which cuts the converter. It shows the fluid dynamic inside the chamber and the heat transfer from the chambers to the external emitting walls, due to the conductive Si-C material.

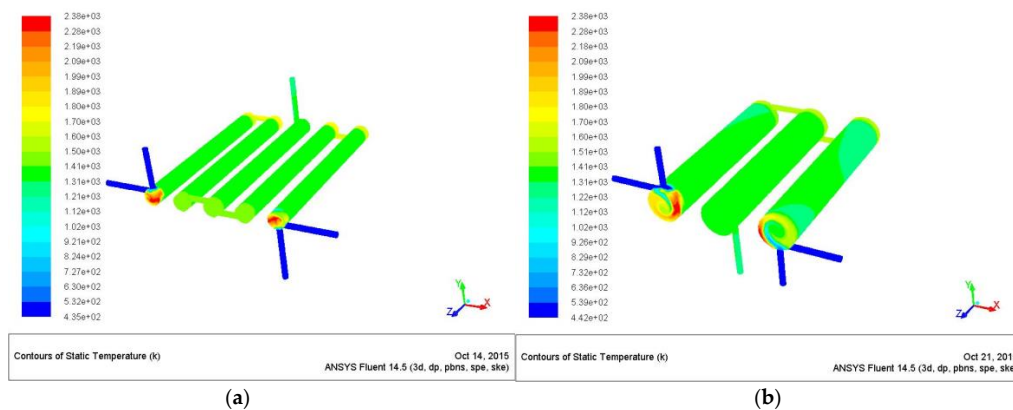


Figure 12. $Z/D = 11$ (a) and $Z/D = 5$ (b), temperature map of the chambers.

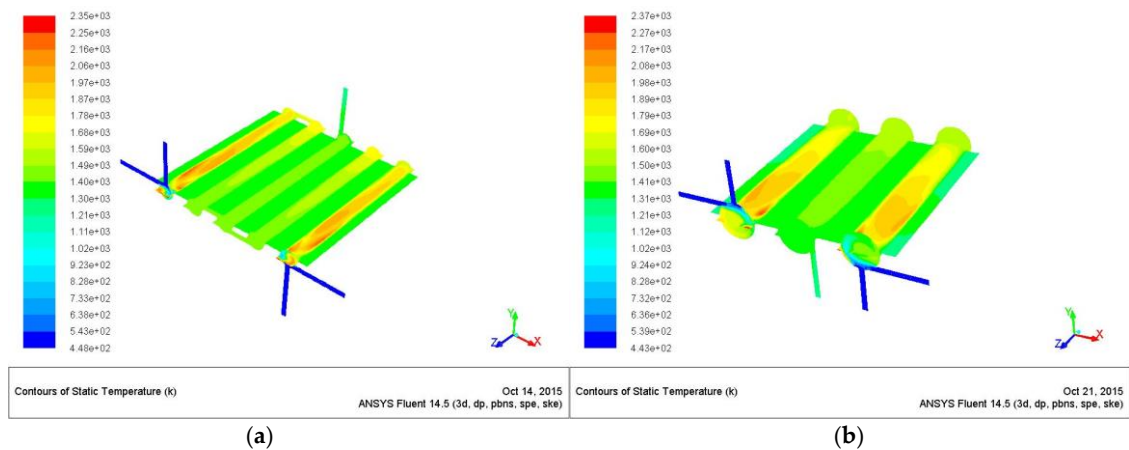


Figure 13. $Z/D = 11$ (a) and $Z/D = 5$ (b), temperature map on the xz-plane.

A burning central zone, where temperature peaks, and a colder zone, close to the wall, are predicted. The centrifugal force, due to the imposed swirling motion, “pushes” fresh reactants toward the wall. This forced stratification naturally protects the wall from the high gas temperature.

Figure 14 reports the temperature map of the emitting surfaces from which it is evident how the configuration with five chambers ($Z/D = 11$) performs better in terms of ΔT . In fact, this configuration figures out an external maximum temperature of 1390 K, and a delta of 45 K, compared to the $Z/D = 5$ configuration that predicts a maximum temperature of 1346 K and a delta of 75 K (see Table 5).

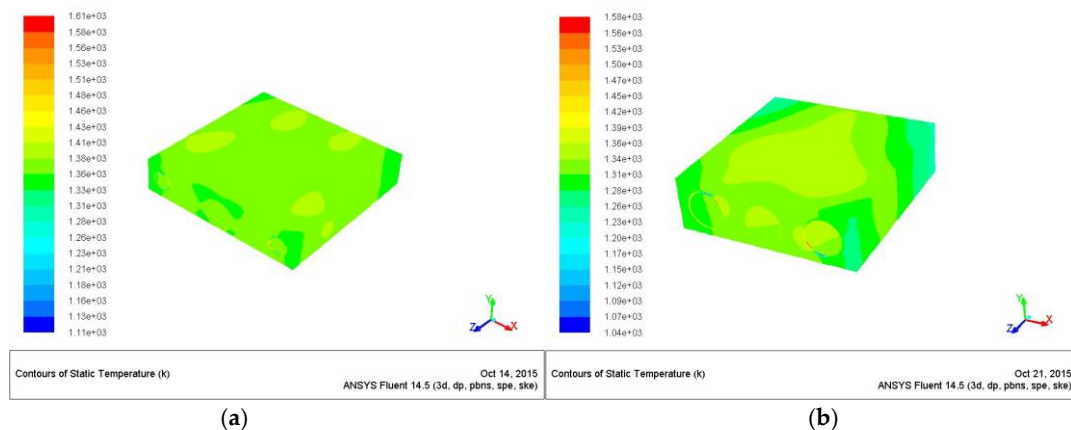


Figure 14. $Z/D = 11$ (a) and $Z/D = 5$ (b), temperature map on the external walls.

Figure 15 provides the overpressure map and shows that an inlet overpressure of about 3 atm, at steady state conditions, is required for both the configurations (the exhaust section is at ambient conditions, $P = 1$ atm). This result differs from what is reported in [1], where the simulation of two “not-connected” chambers, at the same exhaust pressure conditions, predicts a slight overpressure.

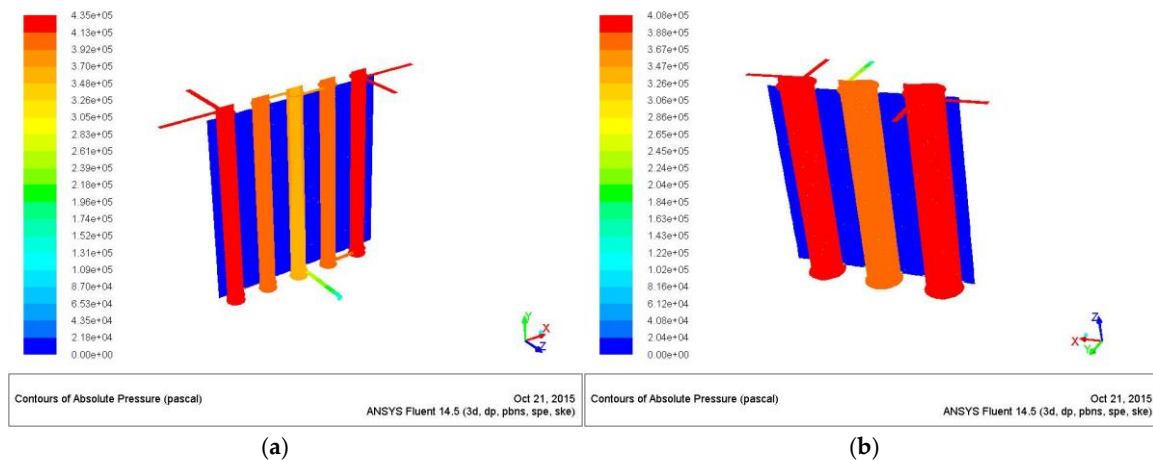


Figure 15. $Z/D = 11$ (a) and $Z/D = 5$ (b), pressure map inside the chambers.

Figure 16 shows the negative Z -velocity maps along the XZ -plane inside the chambers. It shows the recirculation bubbles along the three and five chambers. It is evident how the bubbles are wider in the $Z/D = 5$ configuration than in $Z/D = 11$ one. They work as flame holders and are fundamental for mixing, assuring high chemical efficiencies (values are reported in Table 4).

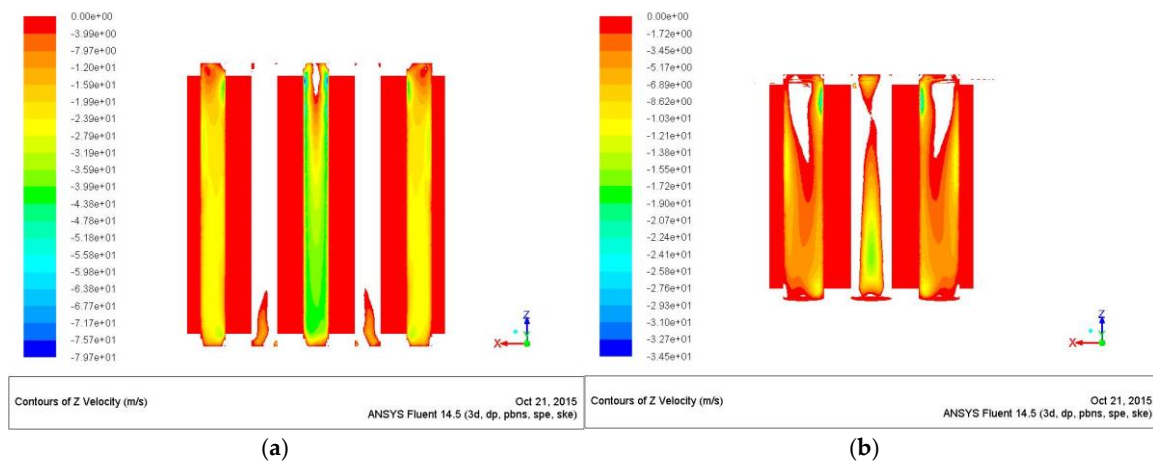


Figure 16. $Z/D = 11$ (a) and $Z/D = 5$ (b), Z -velocity map inside the chambers.

5. Conclusions

This work focuses on the performance of an energy converter characterized by a parallelepiped block of emitting material with internal two, three, and five connected swirling micro-meso chambers, fed by H_2 /air.

These configurations assume identical injected thermal power (500 W) and equivalence ratio ($\Phi = 1$), but differ for the diameter-length ratio, Z/D .

The goal of the work is to define a converter configuration which fulfills, simultaneously, four design requirements: emitting surface area of $30 \times 30 \text{ mm}^2$; a thermal resistance efficiency, during the solar mode, greater than 20%; a peak temperature greater than 1000 K; and the delta temperature on the emitting surface less than 100 K.

These requirements impose, *in primis*, Fourier investigations, to mimic the solar mode operation, and then reactive Navier-Stokes simulations, to reproduce the combustion mode operation.

The Fourier investigation provides that:

- (1) The converter must not exceed a total thickness of 9 mm; and
- (2) The five and three connected chambers ($Z/D = 11$ -3 mm of diameter and $Z/D = 5$ -6 mm of diameter) are the final configurations.

After this, these two configurations are analyzed by means of combustion simulations.

The most important outcomes are:

- (1) Both the configurations provide complete combustion;
- (2) The H_2 chemistry and the great residence time, further increased by the recirculation bubbles due to the swirling movement, are not sensitive to the different geometrical configurations;
- (3) The $Z/D = 11$ performs much better than the $Z/D = 5$ configuration in terms of ΔT and thermal resistance efficiency;
- (4) The counter flows, inside the five combustion chambers, balance the hot-cold points, on the parallelepiped walls, much better than the $Z/D = 5$ configuration; and
- (5) The $Z/D = 11$ configuration is characterized by a more homogenous emitting surface temperature (standard deviation equal to 8 instead of 15) and by a lower surface ΔT (45 K instead of 75 K).

Further improvements might be focused both on numerical and technological issues.

For example, numerically, LES or DNS investigations seem feasible due to the low turbulence levels, at least inside the chambers, while, technologically, cluster configurations and/or connections to micro-turbine, might be analyzed to study the effects on the energy efficiency. In fact, the present results indicate that the temperature at the exhaust section might be compatible with the material requirements at the inlet section of a micro-turbine.

Acknowledgments: European 7th Framework Programme, EU-FP7 ENERGY.2012.10.2.1: Future Emerging Technologies Grant, Hybrid Renewable energy Converter for continuous and flexible Power production (HRC Power) Project.

Conflicts of Interest: The author declares no conflict of interest.

References

1. Minotti, A.; Teofilatto, P. Swirling combustors energy converter: H_2 /Air Simulations of Separated Chambers. *Energies* **2015**, *8*, 9930–9945. [CrossRef]
2. Minotti, A.; Ollier, E. Hybrid Energy Converter Based on Swirling Combustion and Having a Transversal Heat Path. FR15 50448, 20 January 2015. pending patent.
3. Harnessing Hybrids. Pan European Networks. Available online: <http://www.panuropeannetworkspublications.com/st6/#/228/> (accessed on 4 March 2013).
4. Community Research and Development Information Service. Available online: <http://cordis.europa.eu/result/rcn/153340fr.html> (accessed on 4 March 2013).
5. Minotti, A.; Sciubba, E. LES of a meso combustion chamber with a detailed chemistry model: Comparison between the Flamelet and EDM models. *Energies* **2010**, *3*, 1943–1959. [CrossRef]
6. Sui, R.; Prasianakis, N.I.; Mantzaras, J.; Mallyaa, N.; Theilea, J.; Lagrangeb, D.; Friessc, M. An experimental and numerical investigation of the combustion and heat transfer characteristics of hydrogen-fueled catalytic microreactors. *Chem. Eng. Sci.* **2016**, *141*, 241–230. [CrossRef]
7. Minotti, A.; Cozzi, F.; Capelli, F. CH_4 /air Mesocombustor at 3 bar: Numerical simulation and experiments. *Appl. Mech. Mater.* **2013**, *431*, 137–150. [CrossRef]
8. Cuthill, E.H.; McKee, J. Reducing Bandwidth of Sparse Symmetric Matrices. In Proceedings of the Association for Computing Machinery 24th National Conference, New York, NY, USA, 26–28 August 1969; pp. 157–172.
9. Deyer, R.; Zhang, H.; Moller, T. Delaunay mesh construction. In *Eurographics Symposium on Geometry Processing*; Alexander, B., Michael, G., Eds.; Simon Fraser University: Burnaby, BC, Canada, 2007.
10. Shih, T.H.; Liou, W.W.; Shabbir, A.; Yang, Z.; Zhu, J. A New k - ϵ Eddy-Viscosity Model for High Reynolds Number Turbulent Flows. *Comput. Fluids* **1995**, *24*, 227–238. [CrossRef]

11. GRIMech 3.0 Thermodynamic Database. Available online: http://www.me.berkley.edu/gri_mech/version30/files30/thermo30.dat (accessed on 6 December 2015).
12. Anderson, J.D. *Hypersonic and High Temperature Gas Dynamics*; McGraw Hill: New York, NY, USA, 1989; Volume 12, pp. 468–481.
13. Mathur, C.; Saxena, S.C. Viscosity of polar gas mixture: Wilke's method. *Appl. Sci. Res. A* **1966**, *15*, 404–410. [[CrossRef](#)]
14. Magnussen, B.F. On the structure of turbulence and a generalized eddy dissipation concept for chemical reaction in turbulent flow. In Proceedings of the 19th American Institute of Aeronautics and Astronautics Aerospace Science Meeting, St. Louis, MO, USA, 12–15 January 1981.
15. Gran, I.R.; Magnussen, B.F. A numerical study of a bluff-body stabilized diffusion flame. Part 2. Influence of combustion modeling and finite-rate chemistry. *Combust. Sci. Technol.* **1996**, *119*, 191–217. [[CrossRef](#)]
16. Li, J.; Zhao, Z.; Kazakov, A.; Dryer, F.L. An Updated Comprehensive Kinetic Model of Hydrogen Combustion. *Int. J. Chem. Kinet.* **2004**, *36*, 566–575. [[CrossRef](#)]
17. CRESCO: Centro computazionale di RicErca sui Sistemi Complessi. Available online: <http://www.cresco.enea.it/english> (accessed on 6 December 2015).
18. Ponti, G.; Palombi, F.; Abate, D.; Ambrosino, F.; Aprea, G.; Bastianelli, T.; Benoe, F.; Bertini, R.; Bracco, G.; Caporicci, M.; *et al.* The role of medium size facilities in the HPC ecosystem: The case of the new CRESCO4 cluster integrated in the ENEAGRID infrastructure. In Proceedings of the 2014 International Conference on High Performance Computing and Simulation (HPCS 2014), Bologna, Italy, 21–25 July 2014; pp. 1030–1033.
19. Issa, R.I. Solution of implicitly discretized fluid flow equations by operator splitting. *J. Comput. Phys.* **1986**, *62*, 40–65. [[CrossRef](#)]
20. Ferziger, J.H.; Peric, M. *Computational Methods for Fluid Dynamics*; Springer-Verlag: Heidelberg, Germany, 1996.
21. Van Leer, B. Toward the ultimate conservative difference scheme V. A second order sequel to godunov's method. *J. Comput. Phys.* **1979**, *32*, 101–136. [[CrossRef](#)]
22. Thornber, B.; Mosedale, A.; Drikakis, D. On the implicit large eddy simulations of homogeneous decaying turbulence. *J. Comput. Phys.* **2007**, *226*, 1902–1929. [[CrossRef](#)]



© 2016 by the author; licensee MDPI, Basel, Switzerland. This article is an open access article distributed under the terms and conditions of the Creative Commons Attribution (CC-BY) license (<http://creativecommons.org/licenses/by/4.0/>).